The Astrophysical Journal, 840:57 (16pp), 2017 May 1 https://doi.org/10.3847/1538-4357/aa6b02
© 2017. The American Astronomical Society. All rights reserved.

Far-ultraviolet to Near-infrared Spectroscopy of a Nearby Hydrogen-poor Superluminous Supernova Gaia16apd

Lin Yan[1], R. Quimby[2], A. Gal-Yam[3], P. Brown[4], N. Blagorodnova[5], E. O. Ofek[3], R. Lunnan[5], J. Cooke[6], S. B. Cenko[7,8], J. Jencson[5], and M. Kasliwal[5]
[1] Caltech Optical Observatories & Infrared Processing and Analysis Center, California Institute of Technology, Pasadena, CA 91125, USA; lyan@ipac.caltech.edu
[2] Department of Astronomy, San Diego State University, San Diego, CA 92182, USA
[3] Department of Particle Physics & Astrophysics, Weizmann Institute of Science, Rehovot 7610001, Israel
[4] George P. and Cynthia Woods Mitchell Institute for Fundamental Physics & Astronomy, Department of Physics and Astronomy, Texas A. & M. University, 4242 TAMU, College Station, TX 77843, USA
[5] Centre for Astrophysics & Supercomputing, Swinburne University, Hawthorn VIC 3122, Australia
[6] Department of Astronomy, California Institute of Technology, Pasadena, CA 91125, USA
[7] Astrophysics Science Division, NASA Goddard Space Flight Center, Mail Code 661, Greenbelt, MD 20771, USA
[8] Joint Space-Science Institute, University of Maryland, College Park, MD 20742, USA
Received 2016 November 7; revised 2017 March 7; accepted 2017 March 30; published 2017 May 4

Abstract

We report the first maximum-light far-ultraviolet (FUV) to near-infrared (NIR) spectra (1000 Å − 1.62 μm, rest) of a hydrogen-poor superluminous supernova, Gaia16apd. At $z = 0.1018$, it is the second closest and the UV brightest SLSN-I, with 17.4 mag in *Swift* UVW2 band at −11 days pre-maximum. The coordinated observations with *HST*, Palomar, and Keck were taken at −2 to +25 days. Assuming an exponential (or t^2) form, we derived the rise time of 33 days and the peak bolometric luminosity of 3×10^{44} erg s^{-1}. At the maximum, the photospheric temperature and velocity are 17,000 K and 14,000 km s^{-1}, respectively. The inferred radiative and kinetic energy are roughly 1×10^{51} and 2×10^{52} erg. Gaia16apd is extremely UV luminous, and emits 50% of its total luminosity at 1000–2500 Å. Compared to the UV spectra (normalized at 3100 Å) of well studied SN1992A (Ia), SN2011fe (Ia), SN1999em (IIP), and SN1993J (IIb), it has orders of magnitude more FUV emission. This excess is interpreted primarily as a result of weaker metal-line blanketing due to a much lower abundance of iron group elements in the outer ejecta. Because these elements originate either from the natal metallicity of the star, or have been newly produced, our observation provides direct evidence that little of these freshly synthesized material, including ^{56}Ni, were mixed into the outer ejecta, and the progenitor metallicity is likely sub-solar. This disfavors Pair-instability Supernova models with helium core masses $\geqslant 90\,M_{\odot}$, where substantial ^{56}Ni material is produced. A higher photospheric temperature definitely contributes to the FUV excess from Gaia16apd. Compared with Gaia16apd, we find PS1-11bam is also UV luminous.

Key words: stars: massive – supernovae: individual (Gaia16apd)

1. Introduction

UV spectra of supernovae (SNe) provide sensitive probes of the physical state of the ejecta and the environments, including element abundance, kinematic structure, density profile, and ionization state (Panagia 2007; Bufano et al. 2009). Today, a little over 60 SNe have early-time UV spectroscopy, which were taken by *HST*, *Swift*, *IUE*, and *GALEX*. Most of these sources are Type Ia supernova (SN Ia), and a smaller fraction are core-collapsed events. The UV flux from SNe Ia is generally a small fraction of the total emission due to metal-line blanketing (Pauldrach et al. 1996), i.e., almost all of the UV photons initially produced in the inner layers of the ejecta are absorbed by a forest of line transitions from single or doubly ionized iron group elements. These UV observations have instigated a flurry of theoretical studies that examine in detail the effect of ejecta abundance (or progenitor metallicity; Lentz et al. 2000; Mazzali et al. 2014), reverse fluorescence (where ionized iron elements can convert photons from red to blue in the outer layers of ejecta; Mazzali 2000), ionization state (highly ionized iron will produce less UV absorption; Höflich et al. 1998; Sauer et al. 2008), element mixing, and velocity structures of the layers where UV photons are produced (Hillebrandt & Niemeyer 2000). Type II SNe are generally luminous in UV at very early times (minutes to hours after explosion), especially right after the shock wave produced by the core bounce has reached the stellar surface (shock break-out). After shock break-out and during the shock cooling phase, with lower temperature and low ionization state, metal-line blanketing leading to suppression of UV continuum has been observed among SNe Ia and SN IIP (Brown et al. 2007; Dessart et al. 2008; Gal-Yam et al. 2008; Maguire et al. 2012; Pritchard et al. 2014). However, the UV spectra of SNe 1979C and 1980 K from *IUE* have revealed an excess of emission lines from highly ionized species such as N V, N III, and Si IV, which were interpreted as emission from the interaction between ejecta and circumstellar medium (CSM; Panagia et al. 1980; Fransson 1984).

In the past 10 years, one of the new discoveries is SLSN (Quimby et al. 2007; Barbary et al. 2009; Gal-Yam 2012), which is a rare class of SNe that is difficult to explain by standard supernova models. An outstanding question in astronomy is what powers the energetic output from these events. SLSNe are broadly classified into two categories: ones without detectable hydrogen in their early-time spectra (SLSNe-I), and ones with hydrogen and/or helium emission (SLSNe-II or luminous SNe IIn). The characteristics of extreme peak luminosity and very long rise timescale implies that SLSNe may have massive progenitor stars, $>10\,M_{\odot}$ (Nicholl et al. 2015). Optical spectroscopy of SLSNe-I has revealed

features not commonly seen before, such as a series of six O II absorption troughs between 3200 and 4400 Å (e.g., Quimby et al. 2011). These features are likely produced by O^{+} ions with excitation potentials of 25 eV, suggesting a very high temperature radiation field or energetic, non-thermal processes. The relative strength of these O II absorption features in the early-time spectra can vary significantly from object to object. In some cases, only one or two features are visible (i.e., SN2005ap; Quimby et al. 2007; Yan et al. 2017). This could make spectral classification difficult. One example is ASSASN-15lh, whose early-time spectra have only one or two features from this O II series (Dong et al. 2016). This has resulted a very uncertain classification. The physical cause of the spectral difference among SLSNe-I is not yet understood.

Existing UV spectra of superluminous supernovae (SLSNe) are rare, especially for low redshift events. A few rest-frame UV spectra reaching ~2000 Å were obtained for SLSNe at $z > 0.7$ from ground-based optical telescopes. Three characteristic absorption features are observed at 2200, 2500, and 2700 Å. What exact ions produce these features is a topic of debate; whether they are C II, Si II and Mg II as suggested by Quimby et al. (2011) or, C III/C II, C II, and C II/Mg II as proposed by Howell et al. (2013), or identified as C III/C II/Ti III, Ti III/C II/Si II, and C II/Mg II blends by the modeling of Mazzali et al. (2016). The distinguishing power will need to come from the combined spectral data covering far-ultraviolet (FUV), near-ultraviolet (NUV), and optical wavelengths.

Only two FUV spectra exist for SLSNe-I. The first one is a noisy spectrum for PS1-11bam at $z = 1.157$, which was taken with a ground-based optical telescope reaching down to the rest-frame 1300 Å. The second one is from *HST* for ASASSN-15lh, which is a peculiar transient event whose true physical nature is still debated (Brown et al. 2016; Dong et al. 2016; Godoy-Rivera et al. 2016; Leloudas et al. 2016). Clearly, more early-time FUV spectroscopy of SLSNe-I is needed. Furthermore, deeper transient surveys are now capable of detecting SLSNe out to $z > 4$ (Cooke et al. 2012; Tanaka et al. 2013). When these transient candidates are followed-up with ground-based optical spectroscopy, the corresponding spectral features will be in the rest-frame NUV and FUV. Therefore, it is important that we can characterize the basic UV spectral properties of low-z SLSNe.

In this paper, we report the first maximum-light ultraviolet spectra of a bright SLSN-I, Gaia16apd (SN2016eay), at $z = 0.1018$. Our FUV to near-IR (NIR) spectra cover a wide wavelength range from 1000 Å to 16,200 Å (rest-frame). The observed spectral energy distribution (SED) has important implications for high redshift SLSN events. Throughout the paper, we adopt a ΛCDM cosmological model with $\Omega_{\rm M} = 0.286$, $\Omega_{\Lambda} = 0.714$, and $H_0 = 69.6\,{\rm km s^{-1}\,Mpc^{-1}}$ (Planck Collaboration et al. 2016).

2. Observations

2.1. Our Target

Gaia16apd was first discovered as a transient event with *V*-band brightness of 17.3 mag (AB) on 2016 May 16 by the *Gaia* Photometric Survey (Gaia Collaboration 2016). An optical spectrum taken on 2016 May 20 with the Nordic Optical Telescope (Kangas et al. 2016) classified this event as an SLSN-I at $z = 0.1018$ (473 Mpc), making it the second closest SLSN-I among more than 60 discovered to date. Gaia16apd is at the sky position of R.A. = 12:02:51.71, decl. = +44:15:27.4 (J2000). The first *Swift* observation on 2016 May 21 revealed that Gaia16apd is extremely bright in the UV (UVW2, 1928 Å) with a flux density of $2.54 \times 10^{-15}\,{\rm erg\,s^{-1}\,cm^{-2}\,Å^{-1}}$ (17.44 AB mag). Because of its early discovery and the extreme UV brightness revealed by the *Swift* data, we submitted an *HST* Director's Discretional Time (DDT) proposal (PID: 14516) and obtained early-time FUV and NUV spectra. The *HST* COS and STIS UV spectroscopic observations were taken in three epochs on 2016 June 2, 14, and 30 respectively. In addition, optical and NIR spectra were taken at Palomar and Keck around the same time as the *HST* data.

The host galaxy is SDSS J120251.71+441527.4 with u, g, r, i photometry of 22.13, 21.73, 21.76, and 21.19 mag (AB) respectively, which indicates a faint dwarf galaxy. The corresponding absolute magnitudes are −16.11, −16.51, −16.48, −17.05 (AB mag, K-corrected), respectively. For comparison, the Perley et al. (2016) study has shown the median values of M_g and a stellar mass M_* of −17.3 AB mag and $2 \times 10^8\,M_{\odot}$, respectively, based on a sample of 17 SLSN-I host galaxies. This suggests that the host of Gaia16apd is also a dwarf galaxy, which is consistent with other studies of SLSN-I host galaxies (Lunnan et al. 2014; Leloudas et al. 2015; Perley et al. 2016).

Gaia16apd has a Galactic extinction $E(B-V)$ of 0.0132 (Schlafly & Finkbeiner 2011). Adopting $R_V = A_V/E(B-V) = 3.1$ and Cardelli extinction law (Cardelli et al. 1989), we estimate the extinction at 1500 Å is only 0.1 mag, corresponding to less than 10% increase in flux. Dust extinction correction is included in our analysis below.

2.2. Light Curves, Explosion and Peak Dates

The field containing Gaia16apd was also observed by the Palomar Transient Factory (PTF) twice in May and 21 times in April 2016. Unfortunately, Gaia16apd fell on the edge of detector 0 in the images taken on 2016 May 12 and 2016 April 18, as shown in Figure 1. However, we do have enough pixels to perform point-spread-function fitting, and obtained a g-band magnitude of 17.3 ± 0.2 (AB) on MJD = 57520.319 day (2016 May 12). The systematic error in this measurement is very large due to the missing pixels. We used the PTFIDE software to carry out the forced photometry on the reference-subtracted images (Ofek et al. 2012; Masci et al. 2017). No pre-explosion activities were detected between 2012 and 2016 May 12 to a 3σ limit of 21 (AB mag), which is the sensitivity of a single exposure.

The 3σ limit on 2016 April 18 (MJD = 57496.275) is 21.0 mag (AB). From 2016 April 01 to 2016 April 18, there are a total of 21 g-band images from PTF. Stacking the nine images taken between 2016 April 18 and 2016 April 14 (MJD = 57494.2 ± 2 days), the 3σ limit is 21.3 mag (AB). Co-adding all of these images, we obtained 3σ limit of 22.1 mag (AB). This upper limit covers the MJD range of 57487.7 ± 8.5 days. We note that because PTF has over several hundreds of g-band images taken between 2012 and 2016, we are able to make a good reference image. The stacking is done on the reference-subtracted images, and thus the derived magnitude limits are for the supernova only with the host light subtracted.

Gaia16apd was observed by the Ultraviolet and Optical Telescope (UVOT; Roming et al. 2005) on board of the *Swift* observatory (Gehrels et al. 2004) starting on 2016 May 21, at

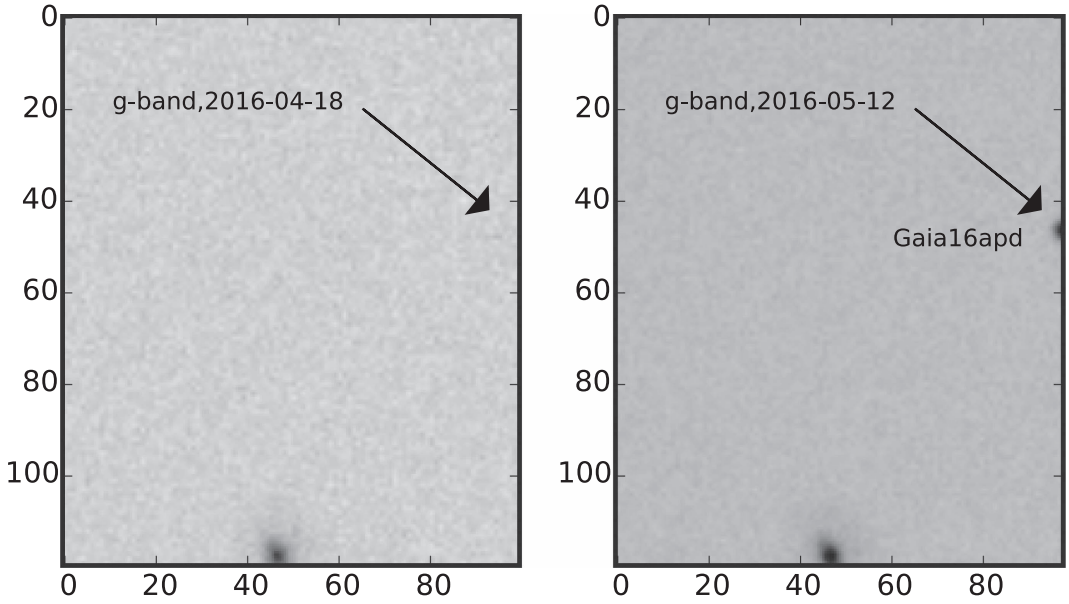

Figure 1. Early-time *g*-band images taken by Palomar 48 inch telescope on 2016 May 12 and 2016 April 18. The axes are in pixels with a pixel scale of 1.″01/pixel. These data allow us to narrow down the explosion date.

an interval of 2–3 days over a month until 2016 June 23. This was the total amount of the approved time from *Swift*. We followed the data reduction outlined for the *Swift* Optical Ultraviolet Supernova Archive (Brown et al. 2014), and the *Swift* photometry calibration is based on Poole et al. (2008) and Breeveld et al. (2010). Table 1 lists all of the broadband photometry included in this paper.

Figure 2 illustrates the monochromatic light curves (LCs) in six *Swift* bands plus optical *g* band. All of the magnitudes here are the total magnitudes without any host galaxy subtraction. It is worth noting that Gaia16apd is extraordinarily bright in *Swift* UV bands. As shown in Figure 2, the highest observed flux in the UVW2 (1928 Å) band is measured as 2.6×10^{-15} erg s^{-1} cm^{-2} (17.5 AB mag) at the first epoch (2016 May 21, MJD = 57529.7 days), which is −11 days before the bolometric peak date. The UV fluxes of Gaia16apd declined only slightly (0.3 mag) between −11 and 0 days when the *HST* UV spectroscopy was taken.

Bolometric luminosities (bottom panel) are the integrals of the blackbody fits to multi-band photometry. For the early times with only *g*-band data, we adopt blackbody temperatures from extrapolation of the multi-band estimates and scale the blackbody curve to match the observed *g* band. One useful parameter is the rise time, $t_{\rm rise} = t_{\rm peak} - t_{\rm exp}$, which is directly related to photon diffusion timescale $t_{\rm diff}$ and ejecta mass estimates (see below). We have $t_{\rm peak} = 57541.4$ days. To determine $t_{\rm exp}$, we use several different methods. One is to assume that an early LC that follows a functional form, for example, an exponential form $L = L_{\rm peak}(1.0 - \exp^{\frac{t_{\rm exp}-t}{t_c}})$ (Ofek et al. 2014), or a power-law form, $L \propto t^2$, like SNe Ia. Although some studies claim that double-peak LCs could be prevalent among SLSNe-I, there is not much concrete observational evidence to support this hypothesis (Nicholl et al. 2015). Since Gaia16apd does not have very early-time photometry, we adopt the assumption of smoothly rising, single-peak profile. With functional fitting, one may naively take the time as the explosion date when luminosity equals zero. Although mathematically this is correct, in practice, this method over-estimates $t_{\rm rise}$. The reason is that just before and after the explosion, the LC could be much steeper than the assumed exponential or power-law forms. Here, we defined the explosion date as when $L \sim 10^5\,L_\odot$, which is the luminosity of a massive progenitor (hot blue supergiant). The fitting used in these two functional forms gives the similar result with $t_{\rm exp} \sim 57505.3$ days and $t_{\rm rise} \sim 33$ days, shown as the dashed line in Figure 2. This is shorter than that of other SLSNe-I published in the literature, although most of these have very few early-time data (Nicholl et al. 2015; A. de Cia et al. 2016, in preparation). Instead of assuming the LC follows certain functional forms, we use the flux limits to constrain the explosion date, shown as the blue dotted line in Figure 2. This yields $t_{\rm exp} \sim 57461.9$ days and $t_{\rm rise}$ of 72 days. The true value of $t_{\rm rise}$ is likely to be smaller than this.

2.3. Spectroscopy: from FUV to NIR

Gaia16apd has an extensive spectroscopy data set at early times. Table 3 summarizes all of the data covering FUV, NUV, optical, and NIR.

The *HST* DDT program was approved for a total of five orbits, with 3, 1, and 1 orbits for the observations taken on UT 2016 June 02 05:08:27, 2016 June 14 04:47:38, and 2016 June 30 03:39:54 UT, respectively. Table 2 summarizes the observation parameters and the key features of the data. The salient point is that the COS FUV spectra cover 1118–2251 Å and the STIS/NUV data are from 1570 to 3180 Å, respectively. The COS and STIS spectra shown below are the reduced products from the *HST* archive.

The optical spectra were taken with the Double Beam SPectrograph (DBSP; Oke & Gunn 1982) on the 200 inch telescope at Palomar Observatory (P200) and the Low-resolution Imaging Spectrometer (LRIS; Oke et al. 1995) on the Keck telescope. The NIR spectra in the *J* and *H* bands were taken with the Multi-Object Spectrometer For Infrared Exploration on the Keck telescope (MOSFIRE; McLean et al. 2012). Table 3 lists the epoch, observatory and instrument, spectral coverage, and resolution for each data set. Optical spectroscopy data are reduced with the software written by E. Bellm (DBSP) and D. Perley (LRIS). The *J*- and *H*-band data were processed by the

Table 1
Photometry[a]

MJD (day)	Filter	Mag (mag)	Error (mag)
57496.275	g	>21.03	…[b]
57520.319	g	17.5	0.1
57529.69	B	16.87	0.045
57529.69	U	16.7	0.036
57529.69	UVM2	17.0	0.042
57529.68	UVW1	16.93	0.042
57529.69	UVW2	17.49	0.042
57529.69	V	16.99	0.071
57531.68	B	16.87	0.054
57531.68	U	16.78	0.045
57531.69	UVM2	17.05	0.042
57531.68	UVW1	17.07	0.050
57531.68	UVW2	17.61	0.042
57531.69	V	17.03	0.091
57533.13	B	16.65	0.063
57533.13	U	16.5	0.045
57533.13	UVM2	17.99	0.050
57533.20	UVW1	16.9	0.050
57533.13	UVW2	17.74	0.058
57533.13	V	16.82	0.11
57537.46	B	16.68	0.054
57537.46	U	16.47	0.045
57537.46	UVM2	17.12	0.042
57537.46	UVW1	16.91	0.042
57537.46	UVW2	17.62	0.042
57537.46	V	16.67	0.071
57541.45	B	16.53	0.045
57541.45	U	16.33	0.045
57541.45	UVM2	17.15	0.042
57541.44	UVW1	16.92	0.042
57541.45	UVW2	17.7	0.042
57541.45	V	16.62	0.071
57543.31	B	16.45	0.045
57543.31	U	16.43	0.045
57543.38	UVM2	17.27	0.042
57543.37	UVW1	16.98	0.050
57543.37	UVW2	17.76	0.050
57543.31	V	16.47	0.071
57545.23	B	16.51	0.045
57545.23	U	16.42	0.036
57545.28	UVM2	17.3	0.042
57545.23	UVW1	17.04	0.050
57545.23	UVW2	17.85	0.042
57545.24	V	16.63	0.071
57547.31	B	16.44	0.045
57547.31	U	16.37	0.036
57547.31	UVM2	17.44	0.042
57547.31	UVW1	17.2	0.042
57547.31	UVW2	17.91	0.042
57547.31	V	16.5	0.061
57550.56	B	16.42	0.045
57550.55	U	16.4	0.045
57550.56	UVM2	17.57	0.042
57550.55	UVW1	17.21	0.042
57550.56	UVW2	18.03	0.042
57550.56	V	16.55	0.071
57556.89	B	16.5	0.045
57556.87	U	16.74	0.045
57556.87	UVM2	17.96	0.050
57556.86	UVW1	17.69	0.058
57556.87	UVW2	18.43	0.058
57556.87	V	16.6	0.071
57559.32	B	16.52	0.045
57559.32	U	16.78	0.045
57559.39	UVM2	18.24	0.05
57559.39	UVW1	17.85	0.06
57559.39	UVW2	18.57	0.06
57559.39	V	16.54	0.08

Notes.
[a] All magnitudes are in AB system.
[b] Errors with … means the photometry is a 3σ upper limit.

MOSFIRE Data Reduction Pipeline.[9] An A0V-type star was observed immediately preceding Gaia16apd and its spectra are used to correct the telluric absorption as well as the flux calibration.

3. Results

3.1. Physical Parameters Derived from the LC

Based on the bolometric LC, the radiative energy emitted over the rest-frame 40 days is $(7 \pm 0.7) \times 10^{50}$ erg. Adopting the photon diffusion approximation and assuming $t_{\rm diff} = t_{\rm rise}$, we have $t_{\rm rise} = \sqrt{2f\kappa M_{\rm ej}/(c \times v_{\rm ej})}$, where $f = \frac{9}{4\pi^3}$ and κ is the mass opacity (Arnett 1996; Padmanabhan 2000). Here, we assume $\kappa = 0.1\,{\rm cm^2 g^{-1}}$, which is commonly adopted for ejecta without H and He. It could be as high as $0.2\,{\rm cm^2 g^{-1}}$ for a fully ionized H-poor medium (Arnett 1982). As shown below, the ejecta velocity $v_{\rm ej}$ can be measured from the optical spectra and is roughly $14{,}000\,{\rm km\,s^{-1}}$. Using the above equation, we have $M_{\rm ej} = \frac{t_{\rm rise}^2\, c\, v_{\rm ej}}{2f\,\kappa}$, thus the estimated ejecta mass $M_{\rm ej}$ is $12\,M_\odot$, with the upper limit of $57\,M_\odot$. This sets the minimum mass of the progenitor star for Gaia16apd. The estimated kinetic energy is roughly 2×10^{52} erg. We note that this method of ejecta mass estimate is extremely crude because the assumption of $t_{\rm diff} = t_{\rm rise}$ could be far-off for power sources other than ^{56}Ni. As discussed in detail in Nicholl et al. (2015), the true diffusion timescale tends to be longer than $t_{\rm rise}$ when central power sources are not ^{56}Ni. This means our ejecta mass is underestimated, and considered as only a lower limit. The proper estimate of diffusion timescale is to use a parametric fitting to the full LC, including an assumed heating function.

3.2. UV Spectra of Gaia16apd

Figure 3 presents the first FUV spectrum of a hydrogen-poor SLSN at a phase of 0 days relative to the peak date (gray—original resolution; green—smoothed). We used a simple boxcar smoothing algorithm from Astropy.[10] Two prominent emission lines are geocoronal Lyα 1216 Å and O I 1302 Å from the upper terrestrial atmosphere. Many narrow absorption lines are present, from both our Galaxy (marked by black lines) and from the host galaxy of Gaia16apd at $z = 0.1018$ (marked by red lines). There are three strong absorption features at the observed wavelengths of 1125, 1190, and 1340 Å, which are not related to the supernova and have been identified as

[9] See http://www2.keck.hawaii.edu/inst/mosfire/drp.html.
[10] http://www.astropy.org

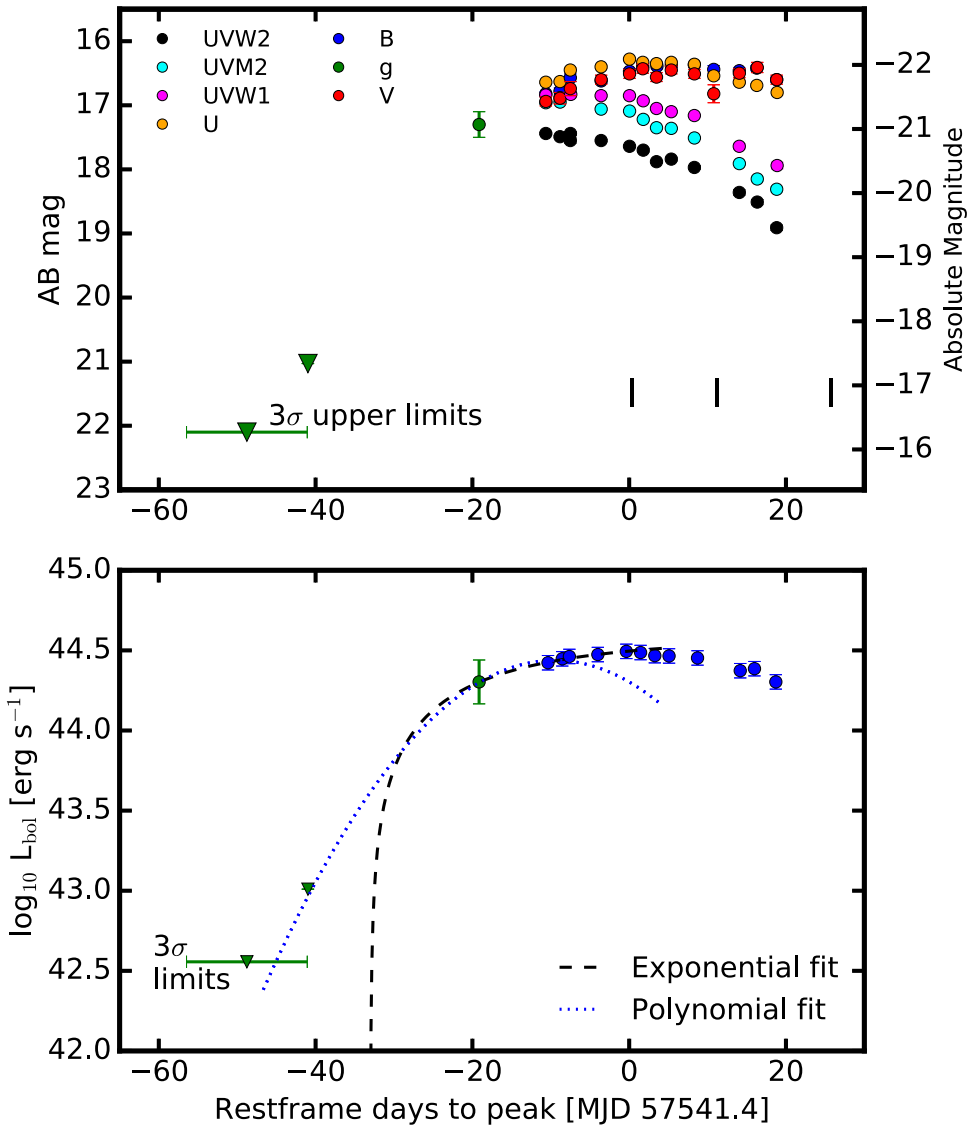

Figure 2. Top panel of this plot shows the early-time monochromatic light curves in various bands, including the limit from Palomar 48 inch telescope. The black vertical bars at the bottom of the top panel mark the dates when the *HST* spectra were taken. The bottom panel is the calculated bolometric light (data points) based on blackbody fits to the broadband photometries. The black dashed line is the exponential fit to the rising portion of the light curve. The dotted line is a 2nd-order polynomial fit to the early-time data. This curve sets the lower limit to the explosion date assuming the slowest rising rate.

Table 2
HST/UV Spectroscopy Observation Log

Obs. UT	No. Orbits	Instrument	Grating	$\Delta\lambda$ (Å)	Spec. Resolution	Obs. Setup
2016 Jun 02 05:22:47	2	COS/FUV[a]	G140L	1118–2251	1500–2900	TIME-TAG
2016 Jun 02 10:06:12	1	STIS/NUV	G230L	1570–3180	500–1010	NUV-MAMA
2016 Jun 14 04:47:38	1	STIS/NUV	G230L	1570–3180	500–1010	NUV-MAMA
2016 Jun 30 03:39:54	1	STIS/NUV	G230L	1570–3180	500–1010	NUV-MAMA

Note.
[a] COST/FUV data was taken using only Segment A.

blended absorption lines from the Milky Way and the host galaxy. Figure 4 presents the zoomed-in version of these three features, with line identifications marked. It is worth noting that the host galaxy of Gaia16apd produces both a damped Lyα absorption, as suggested by the line profile. We also see a weak Lyα emission line from the host as well as Lyβ absorption. This suggests that the SLSN is likely near the inner or backside of the host galaxy in project. Although it is not required by this paper, the host galaxy extinction would be necessary for other studies that require accurate UV luminosities. The wavelength

Table 3
Spectroscopy Observations of Gaia16apd

Date	MJD (day)	Exp. Time (s)	$\Delta\lambda$ (Å)	Spec. Resolution	Instrument
2016 May 27	57535.33	900	3000–9500	1434 at 7500 Å	P200/DBSP
2016 May 30	57538.25	1200	11530–13517	3074 at 11530 Å	Keck I/MOSFIRE
2016 May 30	57538.27	1200	14646–17860	3291 at 14646 Å	Keck I/MOSFIRE
2016 May 31	57539.17	1200	3000–9500	1434 at 7500 Å	P200/DBSP
2016 Jun 02	57541.35	4889	1118–2251	1500 at 1118 Å	COS/FUV/Seg-A/G140L
2016 Jun 02	57541.45	2327	1570–3180	1010 at 3180 Å	STIS/NUV-MAMA/G230L
2016 Jun 07	57546.34	220	3000–10000	1339 at 7500 Å	Keck I/LRIS
2016 Jun 14	57553.21	2327	1570–3180	1010 at 3180 Å	STIS/NUV-MAMA/G230L
2016 Jun 30	57569.12	2327	1570–3180	1010 at 3180 Å	STIS/NUV-MAMA/G230L

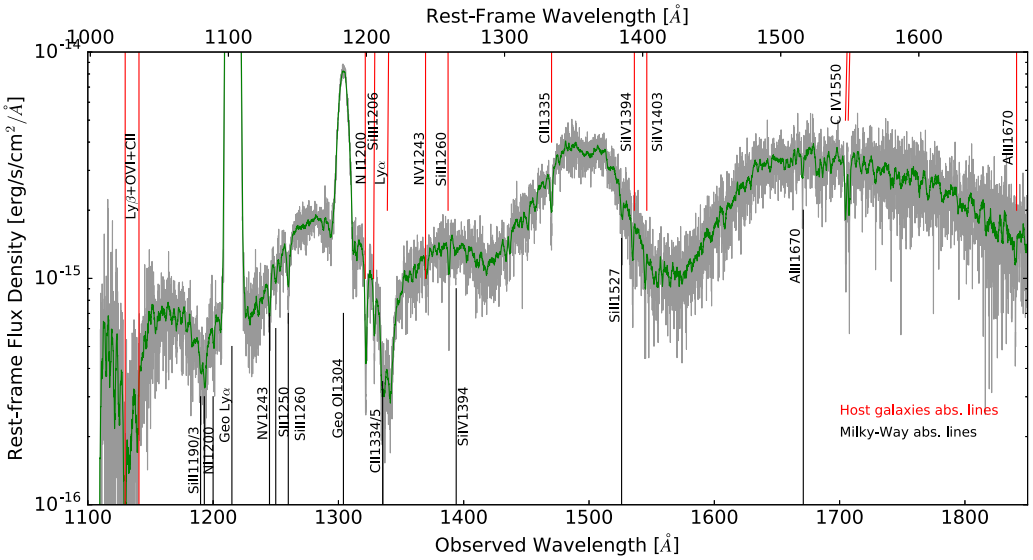

Figure 3. First FUV spectrum of Gaia16apd (SLSN-I) taken with *HST/COS* on 2016 June 02, which is +0 day relative to the peak date. The gray spectrum is the original data and the green line is the smoothed version. The features from the Milky Way are marked with black vertical lines, and the ones from the host galaxy of Gaia16apd are marked with red vertical lines. The *Y*-axis is for the rest-frame flux density in erg s^{-1} cm^{-2}/Å, and the *x*-axis is marked with both the observed (bottom) and the rest-frame (top) wavelength.

of the host Lyα emission line is consistent with that of the host Hβ and Hα emission lines observed in the optical spectra.

In the analyses below, we remove the geocoronal emission lines and the three strong absorption features in order to focus on the broad spectral features due to the supernova Gaia16apd.

3.3. Full SED Near the Peak

One of the main results in this paper is the measurement of the spectral energy distribution (SED) of a hydrogen-poor SLSN, extending from the rest-frame FUV 1000 Å to the NIR 16,200 Å, is shown in Figure 5. This is the first early-time SED for an SLSN-I covering such a wide wavelength range. The SEDs are plotted for three epochs, +0, +11, and +25 days relative to the peak date determined by the *HST* UV observations. The corresponding optical spectra were chosen to match closely with the phases of the UV data (see Table 3 for details). At the maximum light, we need to stitch several spectra together in order to get the full SED. The *HST* UV spectra and *Swift* photometry were taken on 2016 June 02, whereas the closest optical spectrum was taken on 2016 May 31. We convolve the *Swift* broadband filters with the UV and optical spectra. Comparing the calculated magnitudes with that of measured from the *Swift* images, we found that *HST* flux calibration is consistent with that of *Swift* with differences less than 9%, and the optical spectrum taken on 2016 May 31 needs to be scaled down by 11% (i.e., multiplying the optical spectrum by a factor of 0.89). All colors are consistent without any corrections. This small flux correction now matches the optical spectrum to the UV spectra at the correct phase, which was taken on 2016 June 02. Similar cross-checking is also carried out for the second epoch when the *Swift* photometry is available.

All of the spectra, except NIR *J*- and H-band spectra, are plotted as they are; and the *J* and *H* spectra are shifted up by multiplying the original data by a factor of 3.1 and 1.45, respectively. The smaller of these two factors is within the expected calibration uncertainty, and the large scaling factor is because the proper calibration data was missing, and the previous night's calibration observation was used for the *J*-band data. Overall, the SED at the pre-peak phase can be fit by a blackbody with temperature of 17,000 K. At wavelengths short-ward of 2000 Å, the SEDs deviate from a blackbody form, with fewer photons coming through than the blackbody prediction. This is due to some blended line absorption and also a small amount of metal-line blanketing effect. As we argue in the later sections, line blanketing in Gaia16apd is orders of magnitude weaker than that of normal a SN Ia. This reflects

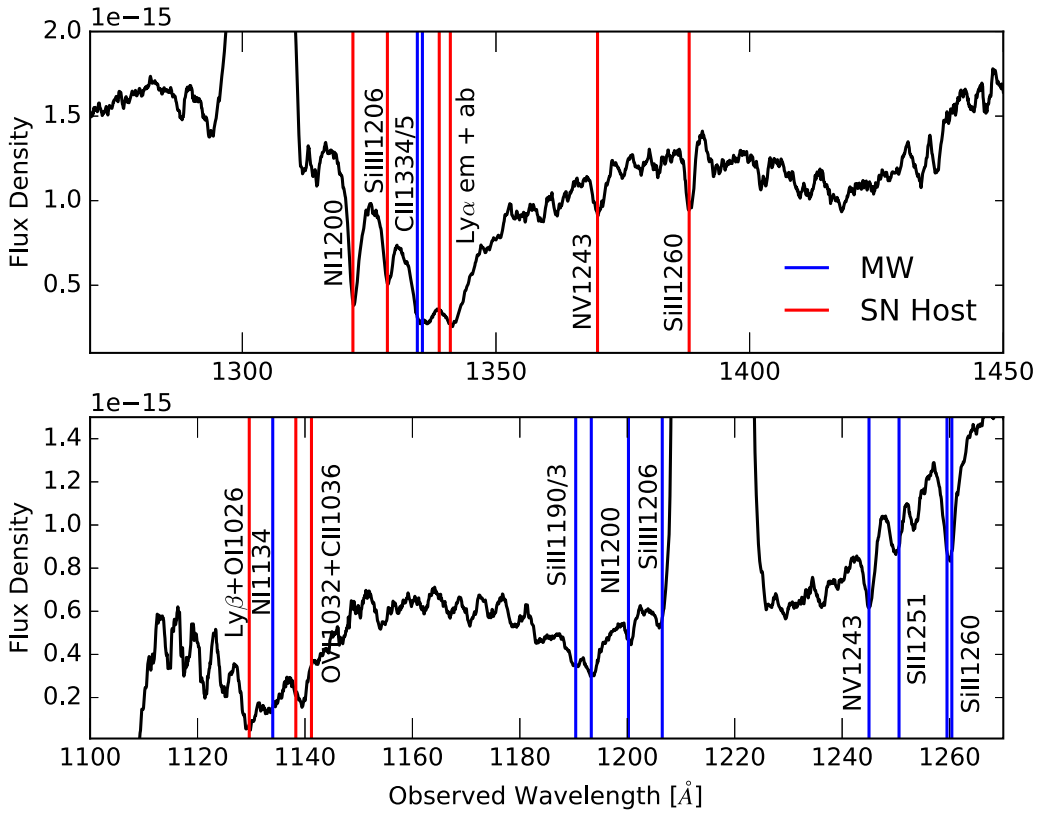

Figure 4. Zoomed-in around the three strong, blended absorption features in the FUV spectra. We show that these three features are not due to the supernova Gaia16apd. The blue vertical lines mark the absorption lines due to the Milky Way, and the red vertical lines mark the lines from the host galaxy.

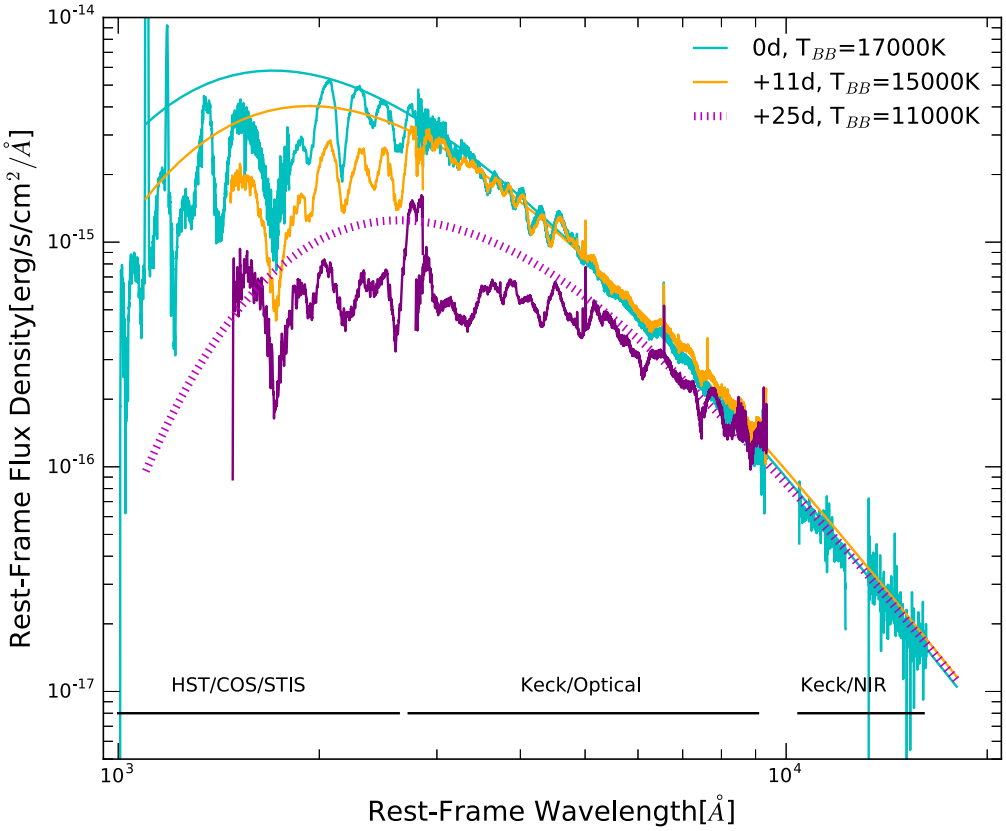

Figure 5. We present all of the early-time spectra taken for Gaia16apd covering the FUV to the NIR. The first epoch (0 day relative to the peak rest-frame) spectra are in cyan, the second epoch (+11 days) in orange, and the third (+25 days) in purple. At the bottom of the figure, we mark the telescopes and instruments used for the observations.

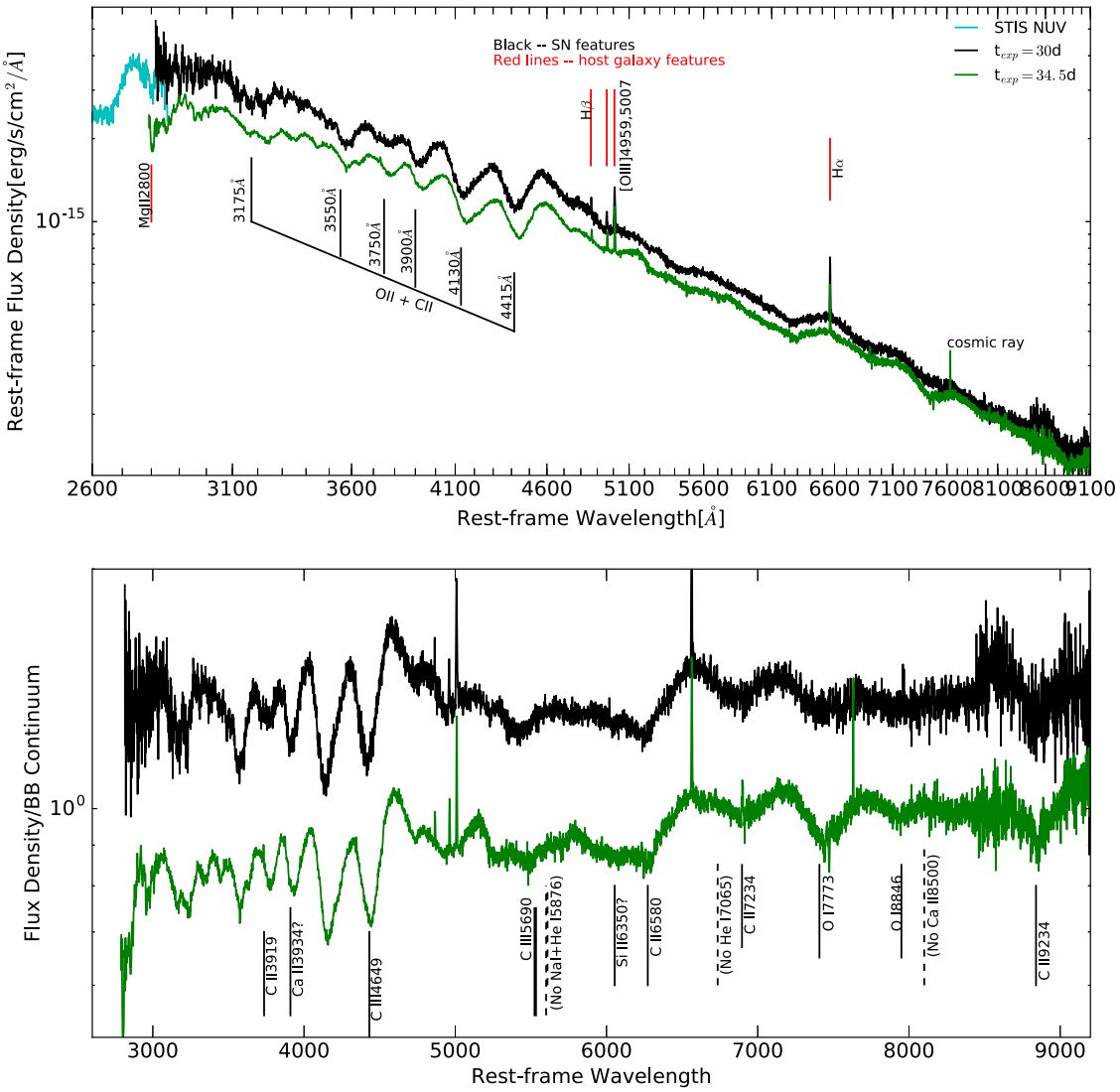

Figure 6. Two optical spectra, taken at the time closest to the first *HST* UV spectra, are presented. The bottom panel shows the spectra with the continuum removed to highlight the rich set of absorption features detected in Gaia16apd. Dashed vertical lines indicate the line transitions, which are expected but not detected in the spectra.

both the absence of newly synthesized heavy elements, as well as intrinsically low metal abundance of the progenitor star (see the detailed discussion below).

The time evolution of the *HST* UV spectra can be summarized as follows. As shown in Figure 5, the blackbody temperatures between the maximum light and +25 day are falling rapidly from 17,000 to 11,000 K. After our paper was submitted for publication, Nicholl et al. (2017) examined the time evolution of the UV spectral features. They found that the equivalent widths of the UV absorption features have become slightly larger with time for Gaia16apd. For this calculation, blackbody fits are adopted as the assumed continua.

We have collected multi-epoch optical spectra for Gaia16apd. The complete analysis of this data set will be presented in a separate paper. Here, we briefly discuss a couple of salient features observed in the early-time optical and NIR spectra. The first epoch *HST* UV spectra were taken on 2016 June 02 ($t_{\rm peak}=0$ day). The two optical spectra near that time were taken on 2016 May 31 ($t_{\rm peak}=-2$ days) and 2016 June 07 ($t_{\rm peak}=4.5$days) with the P200 and the Keck telescopes, respectively. Figure 6 presents these two spectra in both their original form (top panel) as well as the spectra with the blackbody continuum removed (bottom panel). In the top panel, we marked the well-known six O II absorption series (R. M. Quimby et al. 2016, in preparation). The narrow emission lines are [O III]5007 Å, Hβ, and Hα from the host galaxy. These features, in combination with the host galaxy lines in the *HST* spectra, give a precise redshift of 0.1018. Using the minimum of the absorption feature O I 7773, we measure the ejecta velocity of $\sim$14,000 km s^{-1}.

In the bottom panel, we mainly focus on C and O absorption features. We identify C II6580, 7234, 9234 Å, C III4649 (blended with O II series), C III5690 Å, O I7773, and 8446 Å. These C II and C III features are very rarely identified in SLSNe-I except in one case, SN2015bn, where a possible C II was identified by Nicholl et al. (2016). Here, all the features are marked with 14,000 km s^{-1} blueshift. We also marked the positions of two He I features in order to confirm its absence in Gaia16apd. C II7234 Å was detected in SN Ic 2007gr (Valenti et al. 2008), which is thought to be a carbon-rich SN Ic.

Finally, the NIR J and H spectra show mostly continua. Figure 7 displays these two spectra in two panels. One significant spectral line is He I emission line at 1.0833 μm. We believe this He I emission is from the host galaxy, in accord

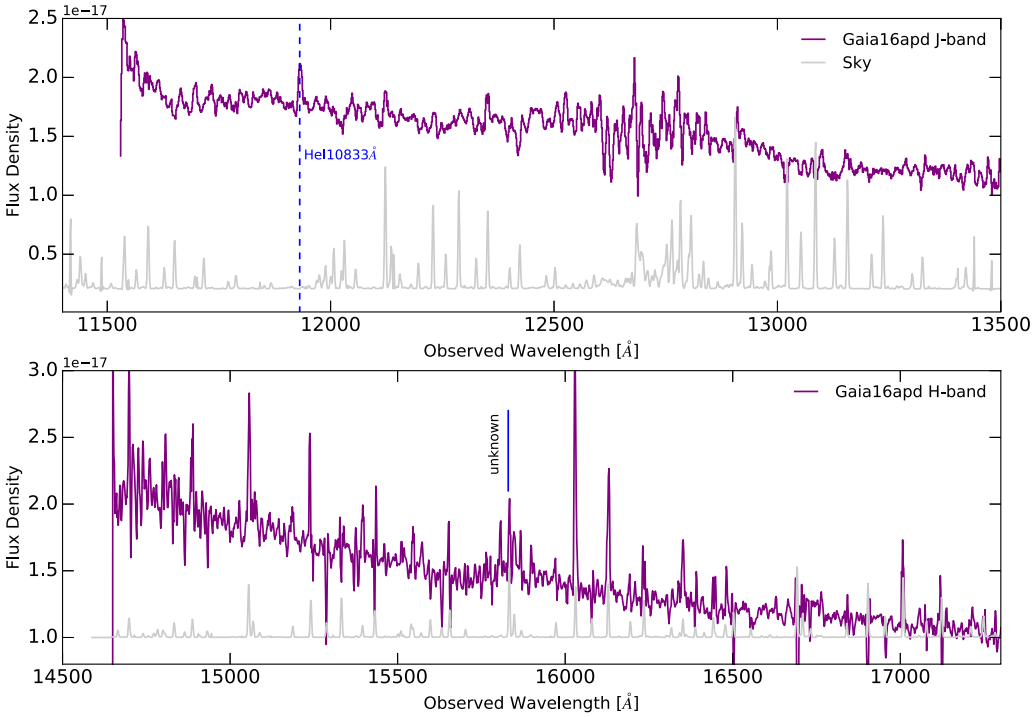

Figure 7. NIR *J*- and *H*-band spectra are presented in the observed frame. In each panel, the J- and *H*-sky spectra, which were taken with the same instrument (MOSFIRE) on the Keck telescope, are plotted in light gray to indicate which regions of the Gaia16apd spectra are free of OH lines.

with other narrow nebular emission lines such as Lyβ, Lyα, Hβ and Hα, which are typical features from low luminosity dwarf galaxies. The lack of He I absorption supports the conclusion that Gaia16apd does not have any He in its optical and NIR spectra. In general, He I 10833 Å is rarely present in the spectra of SLSNe-I. The reported two cases are SN2012il (Inserra et al. 2013) and SN2015bn (Nicholl et al. 2016), where the line identification for SN2012il is very uncertain. The second feature is a broad feature at 15830 Å (observed frame) in the *H*-band spectrum. This feature is in the emission and is fairly weak, which corresponds to the rest-frame 14093 Å. A careful examination of the 2D spectra has confirmed the reality of this feature. However, its physical identification is still a mystery to us. It is very puzzling that, if this feature is associated with Gaia16apd, why it is in emission at the phase of maximum light since most SN spectral features are broad, blended absorption features. If this broad feature were Hydrogen Brackett 14-4 transition at the rest-frame 15884.9 Å, the corresponding observed wavelength centroid would have been much redder at 17502 Å. We carefully checked the telluric correction procedures to ensure this feature is not an artifact introduced during the removal of the telluric absorption feature between 15,700 and 15800 Å. Additionally, this feature is not due to the removal of the nearby Hydrogen Brackett 4–14 absorption feature in the spectrum of the A0V standard used for flux calibrations.

3.4. FUV Excess Emission from Gaia16apd

Figure 8 presents the UV spectrum of Gaia16apd at +0 days, in comparison with that of other SNe with UV spectra normalized at 3100 Å. It is apparent that Gaia16apd is extraordinarily luminous in FUV, and emits 50% of its total luminosity at wavelength <2500 Å, which far exceeds any other normal SN. Figure 8 makes a comparison with the rest-frame UV spectrum of PS1-11bam, which is an SLSN-I at $z = 1.566$ (Berger et al. 2012). Although its signal-to-noise ratio (S/N) is not very high, the rest-frame UV spectrum of PS1-11bam behaves similarly as that of Gaia16apd, with a high fraction of UV emission. This FUV excess from SLSNe-I is further underscored by the comparison with the *HST* UV spectra of normal SNe at early times, including SN 1992A (Ia; Kirshner et al. 1993), SN 2011fe (Ia; one of the closest SNe Ia; Nugent et al. 2011; Foley & Kirshner 2013; Mazzali et al. 2014), SN 1999em (IIP; Baron et al. 2000; Hamuy et al. 2001) and SN 1993J (IIb; Jeffery et al. 1994).

It is well known that SNe Ia have relatively low fluxes in FUV spectra at their maximum light (Maguire et al. 2012). The explanation is that normal SNe Ia produce abundant Fe group elements, including ^{56}Ni, which subsequently goes through β-decay to ^{56}Co ($\tau_{\rm half} = 6.1$ days), then ^{56}Co to ^{56}Fe ($\tau_{\rm half} = 77.7$ days), and releases γ-ray photons that power the observed optical emission. For example, for SNe Ia, the average ejected ^{56}Ni mass is $\sim$0.6 $M_{\odot}$. Single- or doubly-ionized heavy ions are known to have thousands of overlapping line transitions, which strongly absorb the UV photons. This so-called line blanketing effect is the reason why the FUV continuum of an SN Ia is substantially suppressed.

In supernova ejecta, iron-peak elements come from two different channels. One is the intrinsic metal content of the progenitor star. The second source, and more important one, is from newly synthesized material during the explosion. The observed FUV continuum excess in Gaia16apd provides solid evidence that its outer ejecta must not have many iron group elements, including ^{56}Ni. Otherwise, metal-line blanketing would be obvious. If Gaia16apd has any ^{56}Ni, it must be in the inner ejecta; and furthermore, very little mixing happened during the explosion. Late-time observations will be important to confirm this prediction.

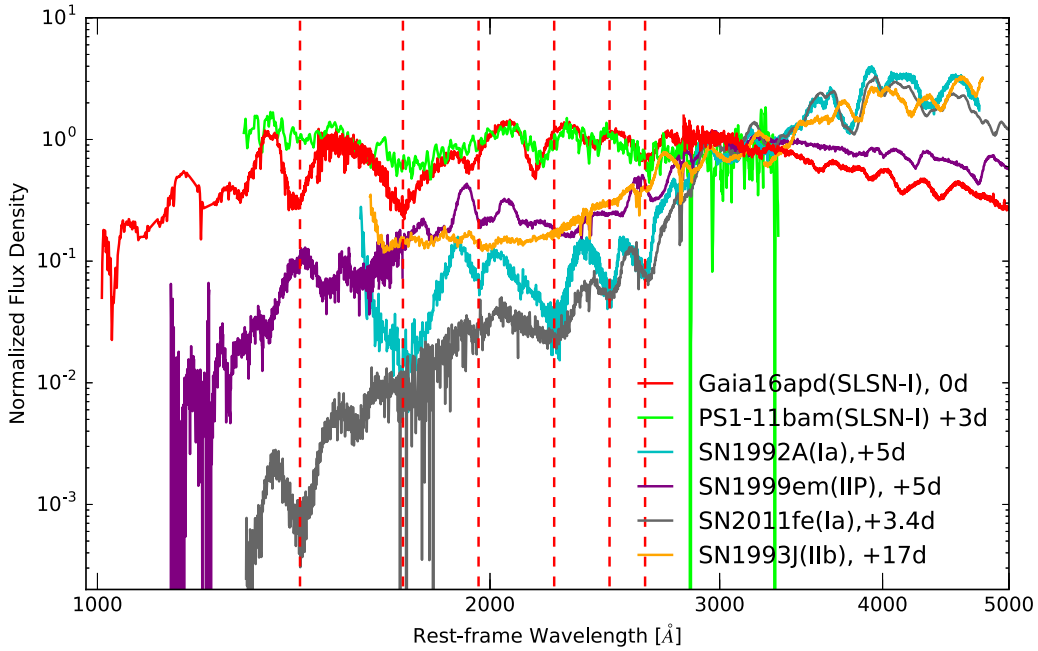

Figure 8. We compared the normalized (at 3100 Å) UV spectra at similar early-phases between Gaia16apd (SLSN-I, red) and the lower luminosity SNe, including SN2011fe (Ia, gray), SN1992A (Ia, cyan), SN1999em (IIP, purple), and SN1993J (IIb, orange). The red dashed vertical lines mark the similar spectral features in both strengths and profiles in Gaia16apd and SN1992A.

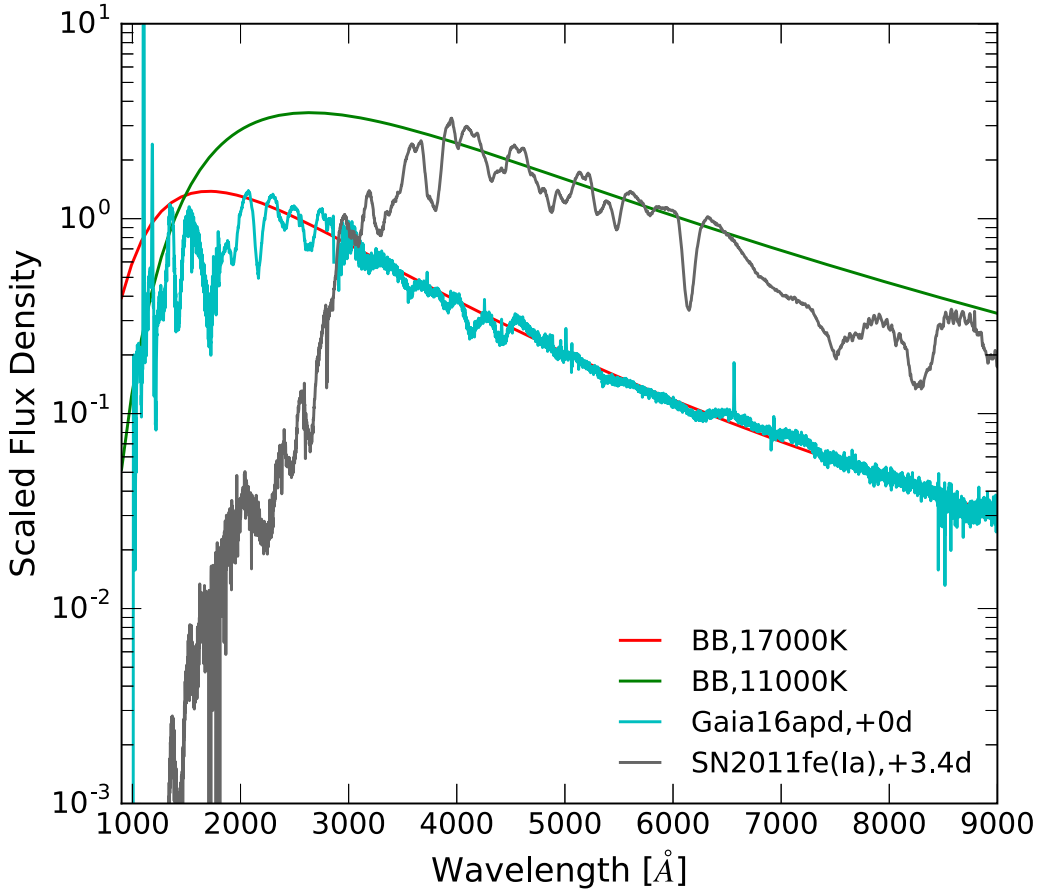

Figure 9. Plot is to illustrate both temperature and line blanketing effects in Gaia16apd and SN2011fe. The line blanketing in Gaia16apd is much weaker than that of SN2011fe. The spectra are normalized at 3000 Å.

Generally, UV spectrum is thought to form in the outer region of the ejecta, where there should be a substantial amount of unburned material, which is directly related to the surface layer of a progenitor star. The apparent lack of strong UV-line blanketing in Gaia16apd also suggests that the metal abundance of its progenitor star is probably sub-solar. For example, Lentz et al. (2000) calculated the metallicity effects in non-LTE model atmospheres of SNe Ia. They found that the model UV spectra can increase fluxes at 1500 Å easily by a factor of 10 when varying metallicity from 1 solar to 1/10 solar (their Figure 2). Their synthetic FUV spectra at 3 and 10 $Z_{\odot}$ show significant line blanketing.

Finally, SLSNe-I tend to have higher photospheric temperatures than that of normal SNe; for example, Gaia16apd has a $T_{BB} \sim 17{,}000$ K, which is about a few thousands degree hotter than that of SNe Ia. So how do we know which factor is the dominant source for the high UV flux in Gaia16apd: weak iron group line blanketing or high photospheric temperature? Figure 9 plots the observed SEDs of Gaia16apd and SN2011fe together with their corresponding blackbody curves. The two spectra are normalized at 3000 Å. This figure shows clearly that line blanketing in SN2001fe is much stronger than that of Gaia16apd, and is the most important reason for its FUV excess. Higher photospheric temperatures do shift overall SEDs toward shorter wavelengths, producing more UV photons. Hotter temperature can also keep more iron group elements at higher ionization states, that contribute less to UV line blanketing. However, the ionization state in Gaia16apd may not be very high because of the detections of weak, low ionization lines such as C II6580, 7234, 9234 Å, and O I7773, 8446 Å in the optical region.

We conclude that the primary reason for the observed FUV excess in Gaia16apd is that its outer ejecta must have very little iron group elements. This rules out the presence of newly synthesized ^{56}Ni, unless it is in the inner region of the ejecta and without any mixing. Furthermore, Our data suggests that the metal abundance of the progenitor star may be sub-solar. These results set very specific constraints on future explosion models.

The strong UV excess and low metal blanketing at maximum light suggest that pair-instability supernova (PISN) model may not work for Gaia16apd. Particularly PISN models with C+O core masses $\geqslant 90\,M_{\odot}$ synthesize a substantial amount of ^{56}Ni (Heger & Woosley 2002). The 33 days rise timescale is too short compared to the PISN model predictions (Kasen et al. 2011), although our estimate has a quite large uncertainty. However, because newly synthesized ^{56}Ni tends to be in the inner parts of ejecta, without mixing, FUV spectra of early-time LCs may show very little absorption by iron group elements. To resolve this ambiguity, we need to follow up with Gaia16apd and its late-time decay slope should determine if ^{56}Ni could be a significant power source. In addition, PISN models with smaller core masses 64–90 $M_{\odot}$ produce very little ^{56}Ni (Heger & Woosley 2002). The main difficulty with this scenario is a lack of power source(s) for the optical LCs. Because PISN models do not produce any compact remnants (no neutron stars and no blackholes), power sources such as magnetars or fall-back blackhole accretion are not available. One could argue that ejecta-CSM (H-poor) or H-poor shell–shell collisions, as predicted by pulsational pair-instability models (Woosley 2016), could provide the energy source. However, the *Swift* XRT observations from +11.6 to −53.6 days yielded no detections, with 90% confidence limits ranging from 6.5×10^{-13} to 1.3×10^{-13} erg s^{-1} cm^{-2} assuming a power-law spectrum with a photon index of +2. The stacked flux limit at 90% confidence is 1.3×10^{-14} erg s^{-1} cm^{-2}, corresponding to the 0.3−10 Kev luminosity of 3.4×10^{40} erg s^{-1}. This limit is about 3×10^{-4} *of* $L_{\rm bol}^{\rm peak}$, an order of magnitude smaller than the predicted by CSM interaction models (Svirski et al. 2012; Ofek et al. 2013). This suggests that interaction is probably not important for this event. Our spectra also rule out the Moriya et al. (2010) models, where energetic core collapse of a $\sim 40\,M_{\odot}$ C+O core could explain the LCs of some SLSNe-I, but these models produce a large amount of ejected ^{56}Ni.

It is worth noting that the PS1-11bam spectrum is similar to that of Gaia16apd with a high UV continuum. This may be an indication that UV luminous SLSNe-I like Gaia16apd could be more common than previously known. However, PTF12dam is a counter example to Gaia16apd. It is an SLSN-I at $z = 0.107$, a similar redshift as that of Gaia16apd. At −11 days, Gaia16apd has a UVW2—V ([1928 Å] - [5430 Å]) color of 17.44-16.99 = 0.45 mag (AB). In contrast, PTF12dam has a UVW2—V color of ∼2 mag (AB) at −20 days (Vreeswijk et al. 2017; Nicholl et al. 2013). This is much redder than that of Gaia16apd, implying that PTF12dam has much less UV flux relative to optical than that of Gaia16apd.

After our paper was posted, Nicholl et al. (2017) has taken our *HST* data and made a comparison with the rest-frame UV spectra at peak or pre-peak phases from other 9 SLSNe-I, including PTF12dam, SN2015bn, SN2010gx, PTF09atu, iPTF13ajg, PS1-10ky, SCP-06F6, SNLS-06D4eu, SNLS-07D2b and PS1-11bam (see their Figure 3). Similar to what we found, Nicholl et al. (2017) concluded that Gaia16apd is indeed a very unique event. Out of a total 10 SLSNe-I, including Gaia16apd, only 3 (33%) have UV excess at 1000–3000 Å similar to that seen in Gaia16apd. Most SLSNe-I (77%) have much less UV emission at 1000–3000 Å, i.e., their UV spectral curves are significantly below that of Gaia16apd. The same comparison was also made at ∼+20 to +30 days post-peak, and shows that all SLSNe-I, including Gaia16apd have similar blackbody temperatures.

In Figure 8, red dashed lines mark six significant UV absorption features. At the first glance, there appears to be some similarity between SN Ia SN2011fe and SLSN-I Gaia16apd, if the blueshifts of some of the features are due to relatively higher photospheric velocity. The question is if these six features are from the same ions. Although detailed spectral identifications based on numerical calculations properly counting all elements and transitions are beyond the scope of this paper, we argue that these features can not come from the same physical transitions. These six features in SN Ia SN2011fe were identified mostly due to iron group elements, blends of Si II+Co II+Fe II (1st), Fe II+Ni II+Co II (4th), Fe II+Co II (5th) and Fe II+Mg II (6th) based on models by Mazzali et al. (2014). These same transitions can not be responsible for all of the UV features from Gaia16apd because it would contradict with the fact that its bright UV emission indicates very little metal-line blanketing. As discussed in Section 3.5, the UV features from Gaia16apd are likely due to intermediate elements, such as Si III, C III, C II and Mg II (Mazzali et al. 2016). Our current theoretical modelings of UV spectra of SLSNe-I are very limited. We can not rule out some

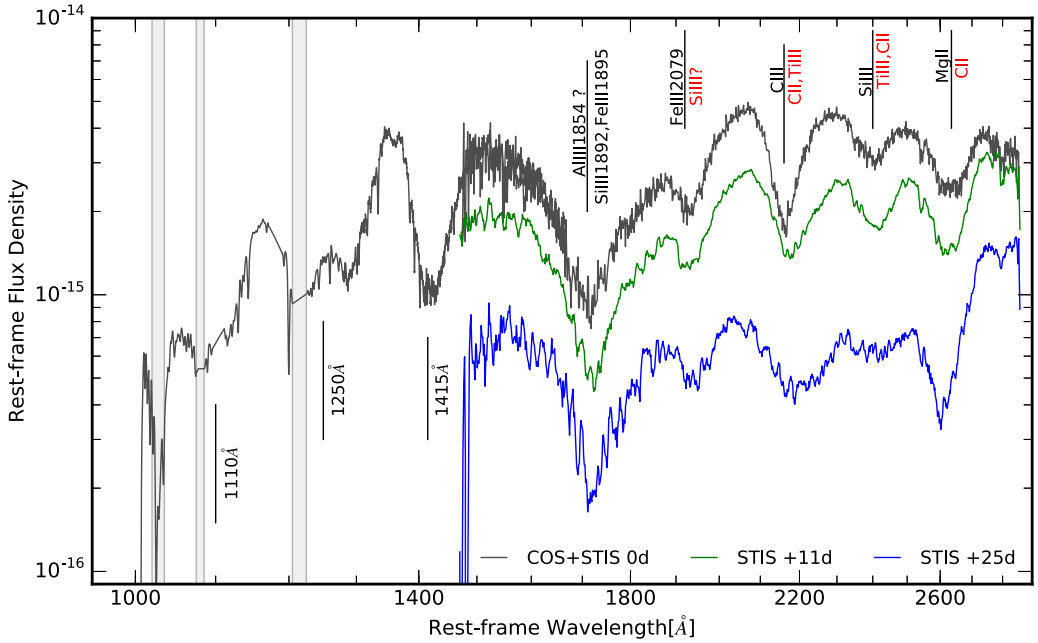

Figure 10. Plot presents the one epoch of FUV spectrum from *HST/COS* at 0 days and the three epochs of NUV spectra at 0, +11, and +25 days relative to the peak. We mark the features we identified based the published papers as well as our own analysis. Three new FUV features are marked with the black vertical lines at 1110, 1250, and 1415 Å. We used the gray vertical bars to mask the regions where deep absorption features are not associated with Gaia16apd, but instead due to the Milky Way and the host galaxy.

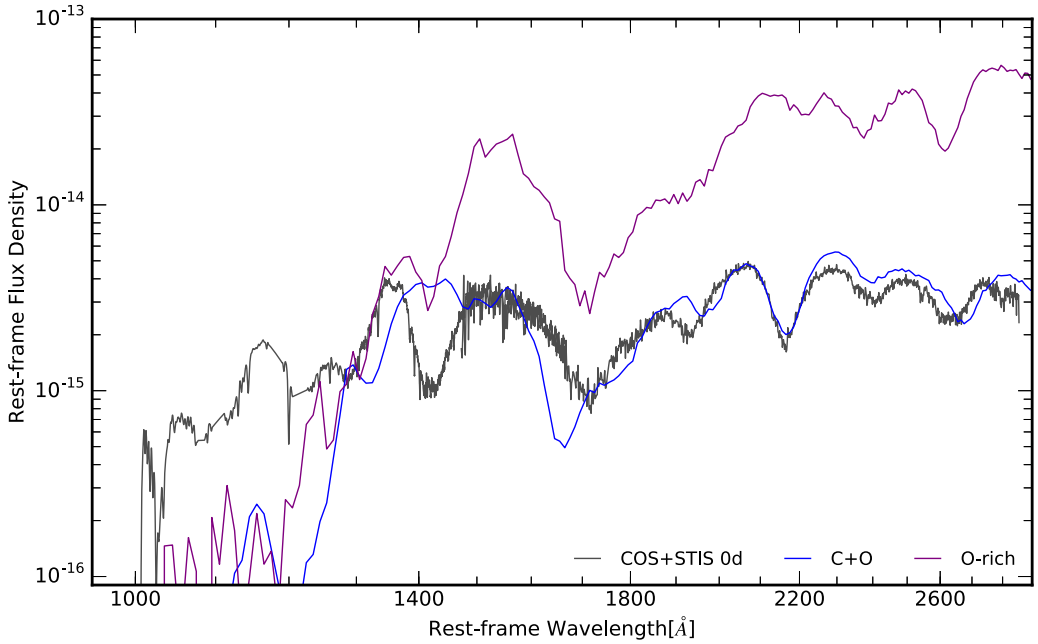

Figure 11. Plot compares our UV spectra at 0 day relative to the peak with two model spectra published in Howell et al. (2013) for two high-z SLSNe-I. The data is in black, the C+O model spectrum is in blue, and the C+O with oxygen-rich is in purple. For the details of the models, see the text.

of these UV features from SLSNe-I and SNe Ia could indeed come from the same physical transitions.

3.5. New UV Spectral Features

Figure 10 presents the FUV and NUV spectra taken at 0, +11 and 25 days relative to optical flux peak using *HST* COS and STIS. Here, we focus only on the features related to the supernova, with other features related to the Milky Way and the host galaxy removed or masked by the gray vertical bars.

The three broad features short-ward of 1500 Å are new and are marked by the black vertical lines. We attempt to shed some light on the feature identifications by comparing with model spectra published for two high-z SLSNe-I in Howell et al. (2013) in Figure 11. These model spectra were calculated for an envelope of an assumed composition above an inner-boundary blackbody using the Monte Carlo radiative transfer code SEDONA (Kasen et al. 2006). The normalization is determined by the assumed ejecta mass $M_{\rm ej} = 5\,M_{\odot}$, kinetic energy $E_{\rm kin} = 10^{52}$ erg, peak bolometric luminosity $L_{\rm peak} = 2.0 \times 10^{44}\,{\rm erg\,s^{-1}}$, and time

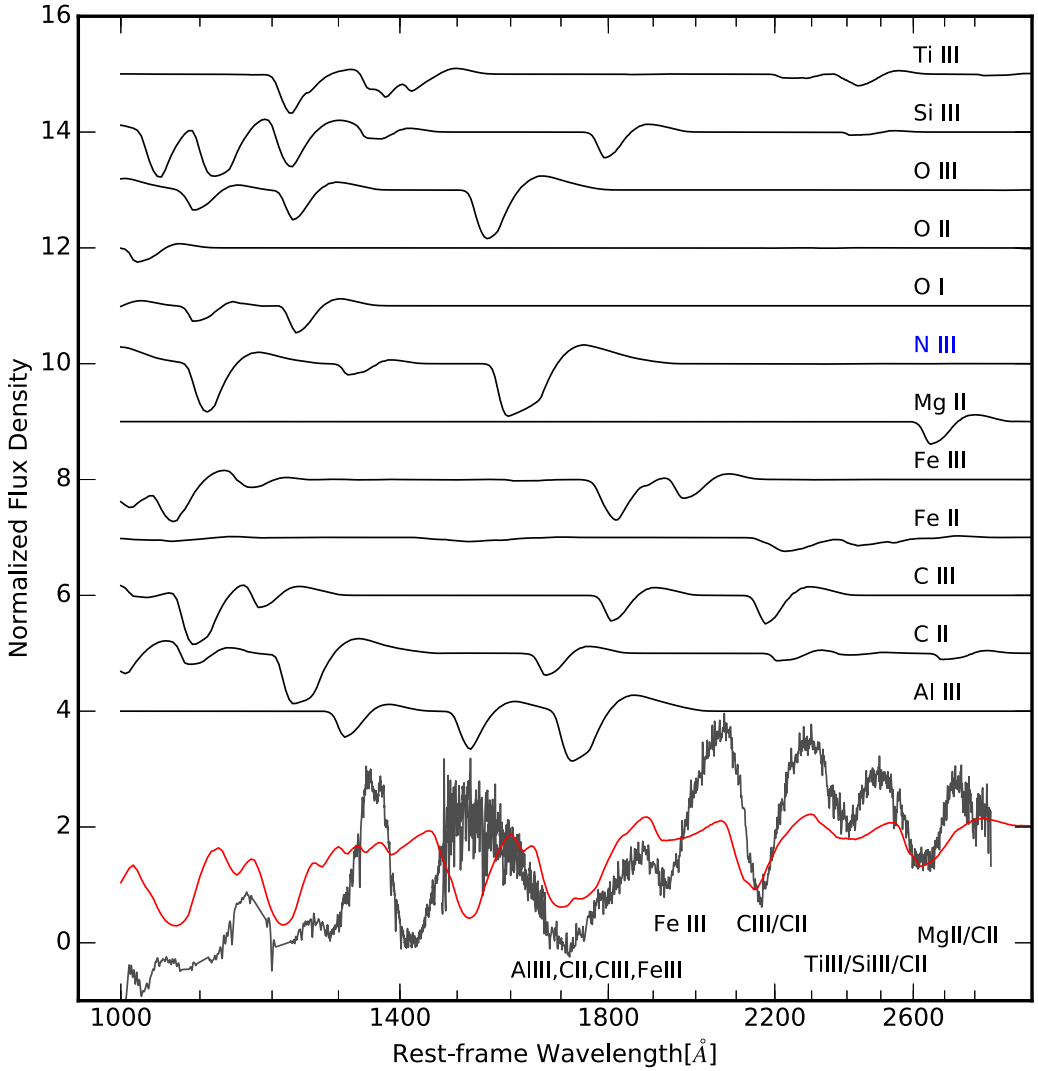

Figure 12. Plot compares the Gaia16apd UV spectra at 0 day with the synthetic spectra generated by syn++ (Thomas et al. 2011). The spectra are normalized and shifted vertically for a clear display. The top 12 spectra were made for each corresponding ion: the bottom black spectrum is the observed data, and the red line is the synthetic spectrum including all of the ions except N III (labeled in blue).

since explosion $t = 25$ days. These parameters are close to those of Gaia16apd, with time t slightly earlier than that of our first UV spectrum (at $t = 30$ days). The two model spectra in Figure 11 are for two different compositions. The blue line is for C+O model where all of the hydrogen and helium in the solar abundance were converted to equal parts of carbon and oxygen, and the purple is for C+O model enhanced in oxygen.

Compared with these two model spectra, the UV spectrum of Gaia16apd clearly has a UV excess. However, the model spectra seem to be able to crudely reproduce some of the observed features, particularly at $\lambda > 1600$ Å. The oxygen-rich model spectrum (purple) seems particularly able to produce most spectral features, but fits poorly to the spectral slope. The metallicities of the model spectra are clearly too high, which under-predicts the FUV fluxes below 1400 Å. It is worth noting that only the oxygen-rich model (purple) seems to be able to explain the newly observed feature at 1400 Å, and the simple C +O model (blue) does not work at all. Although it has been suggested that SLSNe-I are associated with massive C+O cores (Pastorello et al. 2010; Quimby et al. 2011), the FUV spectra from Gaia16apd now provide additional new insights on the properties of the C+O cores of stripped massive stars, which may produce hydrogen-poor SLSNe.

Mazzali et al. (2016) has carried out a modeling of SLSN-I iPTF13ajg spectrum that covers from 1800 to 6000 Å. The three prominent UV features at the rest-frame 2200, 2400, and 2700 Å (4th, 5th, and 6th features marked in Figure 8 respectively) are modeled as blends of C III+C II+Ti III (4th), Si III+Ti III, C II (5th), and Mg II+C II (6th). As shown in Figure 10, the features at 1700 and 1950 Å (2nd and 3rd marked in Figure 8) could be Al III+Si III+Fe III (2nd feature) and Fe III+Si III (3rd) based on the Mazzali et al. (2016) model.

In addition to comparing with the published calculations, we use syn++ code (Thomas et al. 2011) to identify the potential ions producing the observed UV features. The results from this exercise should be regarded as suggestive and by no means a complete nor physically consistent modeling of the data.

Figure 12 shows the comparison between our data and the calculated spectrum for each individual ion, and the combined synthetic spectrum, which including Al III, C II, C III, Fe II, Fe III, Mg II O I, O II, O III, Si III, and Ti III. We exclude N III (marked as blue) from the combined spectrum because this ion

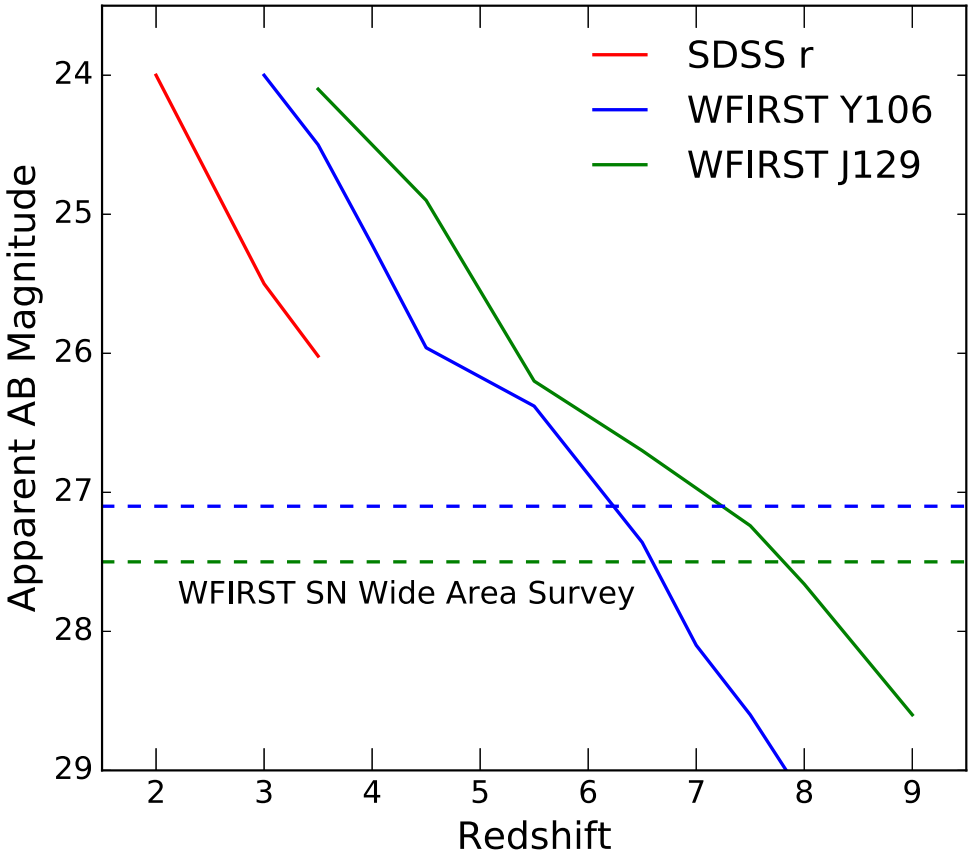

Figure 13. Estimated apparent AB magnitudes at the maximum light for an SLSN-I as a function of redshifts, assuming the same intrinsic SED as we measured for Gaia16apd.

produces a prominent feature near 1600 Å, which causes a strong disagreement with the observed spectrum. We have also calculated spectra for Mn II/III, Co II/III, and Cr II/III; all of these spectra have much weaker features in this region compared to that of Fe II/III.

Of the new features at $\lambda < 1800$ Å, the broad absorption at 1700 Å could be produced by Al III, C II, C III, and Fe III. However, we note that including Al III also produces a strong feature at 1500 Å, which is not present in our data. This implies that even if Al III could contribute to the formation of a 1700 Å feature, it may be small amount. However, none of the ions listed above seem to have a feature at 1400 Å. The spectrum from the O-rich C+O core model (Figure 11, purple) has a narrow absorption feature around 1400 Å. However, this feature was not identified in Howell et al. (2013). In addition, the wavelength region $\lambda < 1400$ Å was not the focus of their paper, and there is clearly too much absorption at the blue end. Improved calculations are clearly needed. The same feature at 1400 Å is also seen in SN Ia SN2011fe (Figure 8). Mazzali et al.'s (2014) paper tentatively identified it as Si II+Co II+Fe II (1st). It is not clear if this same set ions is responsible for the 1400 Å feature in SLSN-I Gaia16apd because its bright UV emission rules out a lot of iron group elements in its outer-layer ejecta. We conclude that to fully understand the observed UV spectra, more theoretical work is needed.

Last, we note that the *HST* UV spectra of Gaia16apd are dramatically different from that of ASSASN-15lh (Brown et al. 2016; Dong et al. 2016; Godoy-Rivera et al. 2016). Since Gaia16apd appears to be a typical SLSN-I, we conclude that ASSASN-15lh's UV spectra are not consistent with the earlier classification as being an SLSN-I. Other interpretations are discussed in the literature (Leloudas et al. 2016; Margutti et al. 2016).

3.6. High-z SLSNe-I

At the maximum light, Gaia16apd has a bolometric absolute magnitude of −22.49, which corresponds to a bolometric luminosity of 3×10^{44} erg s^{-1}. If we assume that all high-z SLSNe-I have the same peak absolute magnitude and UV SEDs similar to that of Gaia16apd at the maximum light, we can easily calculate the apparent magnitude as a function of redshift. Comparing these peak apparent magnitudes with some of the future wide area, time-domain surveys, we can determine if these events at high-z may be detectable. Figure 13 illustrates such a simple calculation, the estimated apparent magnitude in three possible bands, SDSS r for intermediate redshifts, and WFIRST Y106W (0.927–1.192 μm) and J129W (1.131–1.454 μm) filters for high redshifts. One of the main goals of WFIRST is SN Ia Survey, which has two campaigns (each with 5 days cadence for 6 months; Spergel et al. 2015). These two campaigns are 2 yr apart. The WFIRST supernova survey covers 27.4 sq.degree with 5σ sensitivities of 27.1 in Y106W and 27.5 mag(AB) in J129W filters. Therefore, it is promising that we may be able to detect these energetic events out to redshifts of 8.

However, a proper prediction calculation should take into account the peak luminosity and SED distributions. High-z SLSNe-I must follow a distribution of peak luminosities as well as a range of UV SEDs. So far, the observational selection of SLSNe does not have a set of strict criteria. They are commonly selected by peak absolute magnitudes brighter than −20.5 to −21,

followed by spectral classification. Currently, the brightest SLSN-I is iPTF13ajg, with $L_{\rm peak} \sim 6.3 \times 10^{44}$ erg s^{-1} (-23.3 mag; Vreeswijk et al. 2014), and the lower limit of an absolute magnitude of -20.5 corresponds to $L_{\rm peak} \sim 5 \times 10^{43}$ erg s^{-1}. Therefore, Gaia16apd is on the brighter side of the peak luminosity distribution. An unbiased peak luminosity distribution function will require future statistically complete samples.

In addition, as we discussed earlier, at the peak or pre-peak phase, Gaia16apd has many more UV emission than most other SLSNe-I, and its blackbody temperature appears to be higher than that of most other SLSNe-I. This clearly illustrates that the UV SEDs of SLSNe-I are diverse, particularly at peak or pre-peak phases. The real difficulty is constructing a statistically unbiased distribution function. These require analyses are beyond the scope of this paper.

4. Summary and Discussion

The key results from this paper are following. Gaia16apd is one of the closest SLSNe-I ever discovered, only at 473 Mpc. Its proximity and the extreme UV brightness enable us to obtain the first maximum-light UV to NIR spectrum (1000 Å$-$1.62 μm) of an SLSN-I. The high S/N *HST* UV spectra at the maximum light revealed extremely luminous UV continuum, emitting 50% of its total total luminosity at 1000–2500 Å. This is in stark contrast to the UV spectra of other normal SNe, such as SN2011fe (Ia), SN1992A (Ia), SN1999em (IIP), and SN1993J (IIb), where metal-line blanketing of UV photons are significant.

Gaia16apd also has early-time optical images from the PTF before it was triggered as a transient event by the *Gaia* Mission. Our analyses of the photometric LCs infer that Gaia16apd took 33 days to reach its bolometric luminosity of 3×10^{44} erg s^{-1}. Its total radiative energy over the 60 days since its discovery $E_{\rm rad}$ is 1×10^{51} erg. Assuming the photon diffusion timescale to be the same as the rise timescale, the estimated ejecta mass is 12 $M_{\odot}$ with opacity of $\kappa = 0.1$ cm^2 g^{-1}. With the photospheric velocity of $\sim$14,000 km s^{-1} measured from the optical spectra, we calculate the kinetic energy at the explosion $E_{\rm kin} > 2 \times 10^{52}$ erg. This is a powerful event compared to normal SNe, but its kinetic energy is fairly typical for SLSNe.

In UV wavelengths, iron group elements have thousands of lines. FUV photons can be easily absorbed by these transitions and are very sensitive to the presence of these ions. Heavy elements in SNe come from two different sources. One is from freshly synthesized material. Another channel is the intrinsic metal abundance of the progenitor star of a supernova. The observed FUV excess in Gaia16apd has two implications. (1) Its outer ejecta must not have much newly formed iron-peak elements, including ^{56}Ni. If there are any ^{56}Ni, it must be in the inner regions and there is very little mixing. (2) The progenitor of Gaia16apd is a massive star whose metallicity is likely to be sub-solar. We also argue that the high blackbody temperature at the maximum light may also contribute to the FUV excess in Gaia16apd.

Our result clearly rules out PISN models (Heger & Woosley 2002) as well as energetic core collapse models (Moriya et al. 2010). Particularly, the PISN models with progenitor masses $\geqslant$90 $M_{\odot}$ are definitely not viable because in this mass regime, in which a large amount of ^{56}Ni material is produced. The 33 day rise timescale also argues against PISN models because it is quite shorter than model predictions (Kasen et al. 2011).

Although the complete and reliable identification of the UV absorption features requires future detailed modelings, we made a tentative comparison with the published synthetic UV spectra (made available by D. Kasen). This comparison suggests that Gaia16apd may be an explosion of a massive O-rich C+O core with a sub-solar metal abundance. Our high S/N UV spectra have revealed well-detected absorption features, which should set constraints on the chemical composition, ionization state, and temperature of the ejecta modeled by future theoretical studies.

Finally, we utilized our measured SED at the maximum light for Gaia16apd and estimated the apparent peak magnitudes in three different filters for various redshifts. We show that NASA's future NIR space mission WFIRST may provide an opportunity to detect SLSNe-I out to redshift of 8.

We thank Daniel Kasen for very helpful discussion and for making his model spectra available. Vikram Ravi is acknowledged for obtaining some spectra used in this paper. We are grateful to the *HST* staff for the prompt scheduling of these ToO observations. We acknowledge ESA *Gaia*, DPAC, and the Photometric Science Alerts Team.[11] Based on observations made with the NASA/ESA *Hubble Space Telescope*, obtained from the Data Archive at the Space Telescope Science Institute, which is operated by the Association of Universities for Research in Astronomy, Inc., under NASA contract NAS 5-26555. M.M.K. acknowledges support by the GROWTH project funded by the National Science Foundation under PIRE Grant No 1545949. E.O.O. is an incumbent of the Arye Dissentshik career development chair and is grateful for support bygrants from the Willner Family Leadership Institute Ilan Gluzman (Secaucus NJ), Israel Science Foundation, Minerva, and the I-Core program by the Israeli Committee for Planning and Budgeting and the Israel Science Foundation (ISF). A.G.-Y. is supported by the EU/FP7 via ERC grant No. 307260, the Quantum Universe I-Core program by the Israeli Committee for planning and funding, and the ISF, Minerva, and ISF grants, WIS-UK "making connections," and Kimmel and YeS awards. Some of the data presented herein were obtained at the W. M. Keck Observatory, which is operated as a scientific partnership among the California Institute of Technology, the University of California, and the National Aeronautics and Space Administration. The Observatory was made possible by the generous financial support of the W. M. Keck Foundation. The authors wish to recognize and acknowledge the very significant cultural role and reverence that the summit of Mauna Kea has always had within the indigenous Hawaiian community. We are most fortunate to have the opportunity to conduct observations from this mountain.

Facilities: Swift, *HST* (COS, STIS), Keck (LRIS, MOSFIRE), Palomar.

Software: Astropy, SEDONA, syn++.

References

Arnett, D. 1996, in Supernovae and Nucleosynthesis: An Investigation of the History of Matter, from the Big Bang to the Present, ed. D. Arnett (Princeton, NJ: Princeton Univ. Press)
Arnett, W. D. 1982, ApJ, 253, 785
Barbary, K., Dawson, K. S., Tokita, K., et al. 2009, ApJ, 690, 1358
Baron, E., Branch, D., Hauschildt, P. H., et al. 2000, ApJ, 545, 444
Berger, E., Chornock, R., Lunnan, R., et al. 2012, ApJL, 755, L29
Breeveld, A. A., Curran, P. A., Hoversten, E. A., et al. 2010, MNRAS, 406, 1687

[11] http://gsaweb.ast.cam.ac.uk/alerts/home

Brown, P. J., Breeveld, A. A., Holland, S., Kuin, P., & Pritchard, T. 2014, Ap&SS, 354, 89
Brown, P. J., Dessart, L., Holland, S. T., et al. 2007, ApJ, 659, 1488
Brown, P. J., Yang, Y., Cooke, J., et al. 2016, ApJ, 828, 3
Bufano, F., Immler, S., Turatto, M., et al. 2009, ApJ, 700, 1456
Cardelli, J. A., Clayton, G. C., & Mathis, J. S. 1989, ApJ, 345, 245
Cooke, J., Sullivan, M., Gal-Yam, A., et al. 2012, Natur, 491, 228
Dessart, L., Blondin, S., Brown, P. J., et al. 2008, ApJ, 675, 644
Dong, S., Shappee, B. J., Prieto, J. L., et al. 2016, Sci, 351, 257
Foley, R. J., & Kirshner, R. P. 2013, ApJL, 769, L1
Fransson, C. 1984, A&A, 133, 264
Gaia Collaboration 2016, arXiv:1609.04153
Gal-Yam, A. 2012, Sci, 337, 927
Gal-Yam, A., Bufano, F., Barlow, T. A., et al. 2008, ApJL, 685, L117
Gehrels, N., Chincarini, G., Giommi, P., et al. 2004, ApJ, 611, 1005
Godoy-Rivera, D., Stanek, K. Z., Kochanek, C. S., et al. 2016, arXiv:1605.00645
Hamuy, M., Pinto, P. A., Maza, J., et al. 2001, ApJ, 558, 615
Heger, A., & Woosley, S. E. 2002, ApJ, 567, 532
Hillebrandt, W., & Niemeyer, J. C. 2000, ARA&A, 38, 191
Höflich, P., Wheeler, J. C., & Thielemann, F. K. 1998, ApJ, 495, 617
Howell, D. A., Kasen, D., Lidman, C., et al. 2013, ApJ, 779, 98
Inserra, C., Smartt, S. J., Jerkstrand, A., et al. 2013, ApJ, 770, 128
Jeffery, D. J., Kirshner, R. P., Challis, P. M., et al. 1994, ApJL, 421, L27
Kangas, T., Elias-Rosa, N., Lundqvist, P., et al. 2016, ATel, 9071
Kasen, D., Thomas, R. C., & Nugent, P. 2006, ApJ, 651, 366
Kasen, D., Woosley, S. E., & Heger, A. 2011, ApJ, 734, 102
Kirshner, R. P., Jeffery, D. J., Leibundgut, B., et al. 1993, ApJ, 415, 589
Leloudas, G., Fraser, M., Stone, N. C., et al. 2016, arXiv:1609.02927
Leloudas, G., Schulze, S., Krühler, T., et al. 2015, MNRAS, 449, 917
Lentz, E. J., Baron, E., Branch, D., Hauschildt, P. H., & Nugent, P. E. 2000, ApJ, 530, 966
Lunnan, R., Chornock, R., Berger, E., et al. 2014, ApJ, 787, 138
Maguire, K., Sullivan, M., Ellis, R. S., et al. 2012, MNRAS, 426, 2359
Margutti, R., Metzger, B. D., Chornock, R., et al. 2016, arXiv:1610.01632
Masci, F. J., Laher, R. R., Rebbapragada, U. D., et al. 2017, PASP, 129, 014002
Mazzali, P. A. 2000, A&A, 363, 705
Mazzali, P. A., Sullivan, M., Hachinger, S., et al. 2014, MNRAS, 439, 1959
Mazzali, P. A., Sullivan, M., Pian, E., Greiner, J., & Kann, D. A. 2016, MNRAS, 458, 3455
McLean, I. S., Steidel, C. C., Epps, H. W., et al. 2012, Proc. SPIE, 8446, 84460J
Moriya, T., Tominaga, N., Tanaka, M., Maeda, K., & Nomoto, K. 2010, ApJL, 717, L83
Nicholl, M., Berger, E., Margutti, R., et al. 2017, ApJL, 835, L8
Nicholl, M., Berger, E., Smartt, S. J., et al. 2016, ApJ, 826, 39
Nicholl, M., Smartt, S. J., Jerkstrand, A., et al. 2013, Natur, 502, 346
Nicholl, M., Smartt, S. J., Jerkstrand, A., et al. 2015, MNRAS, 452, 3869
Nugent, P. E., Sullivan, M., Cenko, S. B., et al. 2011, Natur, 480, 344
Ofek, E. O., Arcavi, I., Tal, D., et al. 2014, ApJ, 788, 154
Ofek, E. O., Fox, D., Cenko, S. B., et al. 2013, ApJ, 763, 42
Ofek, E. O., Laher, R., Law, N., et al. 2012, PASP, 124, 62
Oke, J. B., Cohen, J. G., Carr, M., et al. 1995, PASP, 107, 375
Oke, J. B., & Gunn, J. E. 1982, PASP, 94, 586
Padmanabhan, T. 2000, in Theoretical Astrophysics: Volume 1, Astrophysical Processes, ed. T. Padmanabhan (Cambridge: Cambridge Univ. Press), 622
Panagia, N. 2007, in AIP Conf. Proc. 937, Supernova 1987A: 20 Years After: Supernovae and Gamma-Ray Bursters, ed. S. Immler, K. Weiler, & R. McCray (Melville, NY: AIP), 236
Panagia, N., Vettolani, G., Boksenberg, A., et al. 1980, MNRAS, 192, 861
Pastorello, A., Smartt, S. J., Botticella, M. T., et al. 2010, ApJL, 724, L16
Pauldrach, A. W. A., Duschinger, M., Mazzali, P. A., et al. 1996, A&A, 312, 525
Perley, D. A., Quimby, R. M., Yan, L., et al. 2016, ApJ, 830, 13
Planck Collaboration, Ade, P. A. R., Aghanim, N., et al. 2016, A&A, 594, A24
Poole, T. S., Breeveld, A. A., Page, M. J., et al. 2008, MNRAS, 383, 627
Pritchard, T. A., Roming, P. W. A., Brown, P. J., Bayless, A. J., & Frey, L. H. 2014, ApJ, 787, 157
Quimby, R. M., Aldering, G., Wheeler, J. C., et al. 2007, ApJL, 668, L99
Quimby, R. M., Kulkarni, S. R., Kasliwal, M. M., et al. 2011, Natur, 474, 487
Roming, P. W. A., Kennedy, T. E., Mason, K. O., et al. 2005, SSRv, 120, 95
Sauer, D. N., Mazzali, P. A., Blondin, S., et al. 2008, MNRAS, 391, 1605
Schlafly, E. F., & Finkbeiner, D. P. 2011, ApJ, 737, 103
Spergel, D., Gehrels, N., Baltay, C., et al. 2015, arXiv:1503.03757
Svirski, G., Nakar, E., & Sari, R. 2012, ApJ, 759, 108
Tanaka, M., Moriya, T. J., & Yoshida, N. 2013, MNRAS, 435, 2483
Thomas, R. C., Nugent, P. E., & Meza, J. C. 2011, PASP, 123, 237
Valenti, S., Elias-Rosa, N., Taubenberger, S., et al. 2008, ApJL, 673, L155
Vreeswijk, P. M., Leloudas, G., Gal-Yam, A., et al. 2017, ApJ, 835, 58
Vreeswijk, P. M., Savaglio, S., Gal-Yam, A., et al. 2014, ApJ, 797, 24
Woosley, S. E. 2016, arXiv:1608.08939
Yan, L. R. Lunnan, et al. 2017, ApJ, submitted